

Self-assembled carbon nitride for photocatalytic hydrogen evolution and degradation of *p*-nitrophenol



Jingwen Sun ^{a,b}, Jingsan Xu ^{b,c}, Andrea Grafmueller ^d, Xing Huang ^e, Clemens Liedel ^b, Gerardo Algara-Siller ^e, Marc Willinger ^b, Can Yang ^f, Yongsheng Fu ^a, Xin Wang ^{a,*}, Menny Shalom ^{b,g,**}

^a Key Laboratory of Soft Chemistry and Functional Materials, Nanjing University of Science and Technology, Ministry of Education, Nanjing 210094, China

^b Department of Colloid Chemistry, Max Planck Institute of Colloids and Interfaces, Research Campus Golm, Potsdam 14424, Germany

^c Ben Gurion University of the Negev, Israel

^d Department of Theory and Bio-Systems, Max Planck Institute of Colloids and Interfaces, Research Campus Golm, Potsdam 14424, Germany

^e Department of Inorganic Chemistry, Fritz Haber Institute of the Max Planck Society, Berlin 14195, Germany

^f State Key Laboratory of Photocatalysis on Energy and Environment College of Chemistry, Fuzhou University, Fuzhou 350002, China

^g Chemistry Department, Ben Gurion University of the Negev, Beersheba 009728, Israel

ARTICLE INFO

Article history:

Received 13 October 2016

Received in revised form 3 December 2016

Accepted 8 December 2016

Available online 9 December 2016

Keywords:

Carbon nitride

Sequential solvent treatment

H₂ evolution

Photodegradation

ABSTRACT

Carbon nitride has attracted significant interest as robust, low-cost alternative to metal-based materials in fields such as photo, electro and heterogeneous catalysis. However, the properties of the final material are hard to control by traditional synthetic methods. Herein, we introduce a new strategy of material design that allows controlling the desired properties of the final material already from the molecular level by sequential solvent treatment of supramolecular aggregates that serve as the reactants. Due to *in situ* formation of a thermodynamic driven energy levels gradient, the as-prepared carbon nitride exhibits almost 10 times higher activity than the traditional carbon nitride (calcined from melamine) in the hydrogen evolution test. As a multifunctional catalyst, the core-shell like carbon nitride also shows a superior catalytic degradation activity for RhB and *p*-nitrophenol.

© 2016 Elsevier B.V. All rights reserved.

1. Introduction

Self-assembly of small molecules by supramolecular interactions is an efficient approach for the formation of well-defined organic crystals, aggregates and other chemical compounds [1–3]. The molecular organization is driven by the creation of non-covalent interactions, i.e., electrostatic, van der Waals interactions, hydrogen bonds and more [4–6]. Among them, hydrogen bonds are very powerful for controlling molecular self-assembly due to their reversibility, specificity, and directionality [7,8]. Melamine, with multiple hydrogen-bonding sites, is extensively applied as a molecular fragment in supramolecular assemblies, especially in combination with cyanuric acid [7]. The cyanuric acid-melamine

complex (CM) is formed by using up to three hydrogen bonds between cyanuric acid and melamine and can adopt various forms, depending on the solvent from which it is aligned and crystallized [9]. Lately it was successfully applied as a precursor for the synthesis of carbon nitride-like materials [8].

As a metal-free semiconductor, graphitic carbon nitride ($\text{g-C}_3\text{N}_4$) materials attracted significant attention in the last years due to their unique chemical, electronic and (photo)catalytic properties [10–15]. The latter depend on the size, morphology, surface area, dispersive ability, light absorption and ability to efficiently separate charges [3,7]. Unfortunately, C_3N_4 , usually possesses limited surface area, difficulty to disperse in solvents and rather low photocatalytic activity [16], if synthesized via traditional routes from simple monomers (cyanamide, melamine, dicyandiamide or urea) [17]. Over the past few years, several templating methods alongside the insertion of other heteroatoms into C_3N_4 structure [18] were introduced in order to increase its performance [19,20]. Due to their unique structural, physical and chemical properties, hollow structures demonstrated especially high activity in the field of photo and heterogeneous catalysis and could also find potential applica-

* Corresponding author.

** Corresponding author at: Chemistry Department, Ben Gurion University of the Negev, Beersheba 009728, Israel.

E-mail addresses: wangx@njust.edu.cn, wxin48@163.com (X. Wang), mennysh@bgu.ac.il (M. Shalom).

tions in drug delivery, catalysis, gas storage, lithium batteries and nanodevices [21].

Up to date, the only way to synthesize metal-free hollow structures is by using soft and hard templating methods [22,23]. However, despite recent progress and a variety of structures that were obtained by the traditional templating methods, they still require multiple steps and are considered relatively complicated and time consuming [4]. Moreover, the template is usually removed by strong acid/base treatment that can damage the organic material.

Recently, we and others demonstrated the advantages of CM supramolecular aggregates that were precipitated from different solvents as the precursors for well-organized C_3N_4 with controllable chemical and photophysical properties [6,8]. The solvent plays a key role for the determination of the aggregations shape, size, etc, alongside the strength and types of the supramolecular interactions due to thermodynamic and kinetic factors. The solubility of the starting monomers, the supramolecular interactions of the solvent with the monomers and the thermodynamic stability of the formed aggregates will govern the aggregation process. Hence, the morphology of CM aggregates as well as the morphology, photophysical and catalytic properties of the final C_3N_4 are strongly depended on the solvent from which the CM was arranged [24–26]. While the role of the solvent in the creation of supramolecular aggregates followed by the formation of ordered C_3N_4 -like materials is partially known, the influences of additional solvent treatment on the supramolecular interactions and on the shape of these aggregates are less explored [27–29]. Furthermore, to the best of our knowledge, the use of the modified supramolecular complexes as the carbon nitride precursor has not been explored before.

Herein, we show the synthesis of highly photoactive carbon nitride hollow structures by altering the properties of the starting CM supramolecular aggregates upon sequential solvent treatment. The influence of the second solvent on the supramolecular assemblies is intensively studied. Our results show that the second solvent can lead to a full rearrangement of the CM structure or only modify the aggregate surface while preserving the bulk morphology, depending on the solvent polarity. The latter results in the creation of different supramolecular crystals along the assembly. The alteration of the hydrogen bond strength across the assembly leads to a difference in the reactivity of inner and the outer crystal upon heating at high temperatures. To investigate the growth mechanism and solvent effect, the chemical structure, morphology and optical properties of the resulting carbon nitrides are characterized by XRD, FT-IR, SEM, TEM, optical microscopy, XPS, UV-vis absorption and steady-state fluorescence spectroscopy. *In-situ* heating experiments are conducted by TEM and light microscopy under controlled conditions, revealing the growth mechanism of the hollow structures at high temperature. The photocatalytic activity is tested by measuring the H_2 evolution and the degradation of Rhodamine B (RhB) dye and *p*-nitrophenol (*p*-NP) under illumination in the presence of the resulting C_3N_4 s.

2. Experimental

2.1. Synthesis of C_3N_4

Microsized mesoporous carbon nitride was prepared via simple calcinations of CM aggregates (with 1:1 molar ratio of cyanuric acid and melamine) at 550 °C for 4 h at a heating rate of 2.3 °C min⁻¹ in a nitrogen atmosphere. In a typical synthesis, 0.5 g of cyanuric acid and 0.5 g of melamine were separately well dissolved in 10 mL and 25 mL DMSO, respectively. Both solutions were mixed for 1 h via an automatic shaker. The precipitate after centrifugation is named CM-D. After addition of H_2O (1:1, v:v, respective to DMSO), the

dispersion was mixed and shaken for another 20 h. The white powder, after centrifuge and drying, is denoted as CM-D1H2O. After calcination in nitrogen atmosphere at 550 °C, the yellow corresponding carbon nitride is named CN-DH. To analyze the formation mechanism of differing morphologies of C_3N_4 , the aforementioned procedure was also applied with different solvents and mixing times (H_2O , MeOH, EtOH, acetone) as indicated in the paper. Carbon nitride calcinated from melamine only was named as bulk.

2.2. Theoretical calculation

Molecular Dynamics (MD) Simulations were performed for melamine and cyanuric acid in all solvents, using Force field parameters obtained from the database [30] for melamine, cyanuric acid, and solvent boxes of ethanol, methanol and acetone [31]. For DMSO, parameters and solvent box from Supplementary Refs. 5 and 6 respectively were used [32,33]. Simulations were started using single solute molecules or small aggregates of one ring, or three stacked rings of 6 solute molecules constructed the crystal structure of melamine-cyanuride [34]. The structures were solvated with the different solvents and simulated using the gromacs software [35]. The systems were equilibrated for 20 ns using weak coupling, and then simulated for 50 ns with a 0.002 ps time step at constant temperature of 310 K and constant pressure of 1 bar, controlled by the Nose-Hover Thermostat and Parrinello Rahman barostat, respectively. Electrostatics were calculated using the particle mesh ewald method [36]; bonds involving hydrogen atoms were constrained using LINCS [37]; water molecules were kept rigid with SETTLE [38]. In the analysis, h-bonds were determined using a cut-off radius of 3.5 Å and angle of 30°.

2.3. Hydrogen evolution test under white LED

Reactions were conducted in a side-irradiated closed steel reactor equipped with a Teflon inlet, thermocouple, pressure sensor, magnetic stirring and thermostat, and connected to a Schlenk line. 30 mg of catalyst was dispersed in 38 mL of the solvent mixture composed of triethanolamine (TEOA) and water in the ratio of 1:9 (v:v). Pt nanoparticles were deposited on carbon nitrides from hexachloroplatinic acid (H_2PtCl_6) via *in situ* photodeposition method. The build-up of H_2 pressure was monitored as a function of the irradiation time (with a white LED array). The headspace of the reactor was also analyzed with mass spectrometry (Pfeiffer Vacuum Thermo Star GSD 301 T gas analyzing system; using argon as carrier gas), confirming the evolved gas as hydrogen.

In addition, the apparent quantum yield (AQY) for H_2 evolution was also measured using monochromatic LED lamps with band pass filter of 420 ± 4.6 nm (the output section was shown in equation below, errors of wavelength were depended on Gauss Simulation of full width at half maximum), the intensities was 14.3 mW cm⁻² (ILT 950 spectroradiometer). The irradiation area was controlled as $3 \times 3 \text{ cm}^2$. Depending on the amount of hydrogen produced by the photocatalytic reaction in an average of one hour, and the AQY was calculated as follow:

$$\eta_{\text{AQY}} = \frac{N_e}{N_p} \times 100\% = \frac{2 \times M \times N_A}{E_{\text{total}}/E_{\text{photon}}} \times 100\% \\ = \frac{2M \times N_A}{\frac{S \times P \times t}{\hbar \times c}} \times 100\% = \frac{2M \times N_A \times \hbar \times c}{S \times P \times t \times \lambda} \times 100\% \quad (1)$$

Where, M is the amount of H_2 molecules (mol), NA is Avogadro constant ($6.022 \times 10^{23} \text{ mol}^{-1}$), \hbar is the Planck constant ($6.626 \times 10^{-34} \text{ Js}$), c is the speed of light ($3 \times 10^8 \text{ m s}^{-1}$), S is the irradiation area (cm^2), P is the intensity of irradiation light (W cm^{-2}), t is the photoreaction time (s), λ is the wavelength of

the monochromatic light (m). Further experimental details and characterization are given in the Supplementary Information.

2.4. Degradation of RhB under white LED

The photocatalytic activity was evaluated by the degradation of Rhodamine B (RhB) under white light irradiation. In a typical photocatalytic degradation experiment, RhB aqueous solution (5 mL, 10 mg L⁻¹) and carbon nitride (5 mg) were mixed in a glass bottle in dark with continuous stirring for 30 min at room temperature to reach the adsorption–desorption equilibrium between the dye and the catalyst. At a given time interval of irradiation, aliquots were withdrawn from the suspension, and all the catalyst was removed. The concentration of the remnant dye was spectrophotometrically monitored by optical absorption values (at 554 nm of UV–vis absorption spectra) on an ultraviolet-visible spectrophotometer during the photodegradation process.

2.5. Degradation of p-NP under UV light

A 500 W Hg lamp was used as the light source. In a typical p-NP (*p*-nitrophenol) degradation experiment, *p*-NP aqueous solution (30 mL, 10 mg L⁻¹) and carbon nitride (3 mg) were put in a quartz tube and then placed in dark with continuous stirring for 30 min at room temperature. After the adsorption–desorption equilibrium, turned on the light. At a given time interval, aliquots were withdrawn from the suspension, and all the catalyst was removed. The concentration of the remnant *p*-NP was spectrophotometrically monitored by optical absorption values (at 317 nm of UV–vis absorption spectra) on an ultraviolet-visible spectrophotometer during the photodegradation process.

3. Results and discussion

3.1. Formation of CM supramolecular aggregates

Supramolecular aggregates were synthesized by mixing a 1:1 molar ratio of cyanuric acid and melamine in a variety of solvents and then centrifuged and dried at 60 °C overnight. The cyanuric acid and melamine complex is created by using up to three hydrogen bonds between cyanuric acid and melamine and can adopt various forms, depending on the solvent from which it is aligned and precipitated (Supplementary Scheme S1). Reactions in dimethyl sulfoxide (DMSO) were carried out for 1 h, whereas experiments in H₂O, ethanol (EtOH), methanol (MeOH) and acetone were allowed to proceed for longer (20 h) due to the lower solubility of cyanuric acid and melamine in these solvents. Differences in the monomer solubility and solvent–monomer interactions, which can straightly influence the direction of hydrogen bond growth, lead to various morphologies of the resulting aggregates. The morphology of CM from DMSO (CM-D) resembles uniform spheres composed of small crystals with an average diameter of 3 μm (Supplementary Fig. S1a). For CM from water (CM-H), a rod-like morphology was observed, while the use of EtOH (CM-E) resulted in a flower-like morphology (Supplementary Fig. S2a,b) [8]. In MeOH or acetone, the shapes of CM aggregates (CM-M and CM-A, respectively) were mostly irregular (Supplementary Fig. S2c,d). Further investigations of the CM formation were conducted by using XRD and FT-IR (Supplementary Fig. S2e,f).

To further understand the solvent effect on the strength of hydrogen bonds within the aggregates and how the solvent influences their shapes and chemical properties, the CM aggregates prepared from DMSO were sequentially transferred to another solvent with different polarity (H₂O > MeOH > EtOH > acetone) and mixed for several hours (labeled as CM-D1Hx, CM-D1Mx, CM-D1Ex

and CM-D1Ax, respectively, with “1” indicating 1 h complex formation time in DMSO and “x” indicating the time in hours of treatment with the second solvent). The introduction of water to CM-D results in a structural collapse from spheres to rods and crystals after 20 h, which is kinetically governed (Supplementary Figs. S1 and S3a–d). The new assembly was confirmed by XRD and FT-IR measurements (Supplementary Fig. S3e–f). Notably, in comparison to CM-D, a new diffraction peak around 11.9° evolves with increasing reaction time for the CM-D1Hx, possibly due to the different in-plane rearrangement of the CM monomers.

In the same way, we explored the influence of less polar solvents on the supramolecular complexes by immersing the CM-D in MeOH, EtOH and acetone. In contrast to H₂O treatment, the original sphere-like morphology is maintained after mixing in the additional solvent for 20 h. The surface of the spherical particles, however, changes to sheet- or stick-like morphologies (Fig. 1a–f). The stability of the hydrogen bond complexes is confirmed by FT-IR and XRD measurements (Supplementary Fig. S4).

Our observations indicate a mechanism in which the second solvent can either induce rearrangement of the supramolecular aggregate or only act as a surface modifier. Crystallization processes of supramolecular aggregates are relatively complicated and controlled by both thermodynamic (the creation of the most stable crystal) and kinetic factors (the formation of the first nucleation seed and the solubility of the monomers). In addition, the properties of the solvent (solubility of monomers, polarity) will dramatically influence the rearrangement process. In our case, we started with uniform spherical particles that were formed by supramolecular self-assembly in DMSO. In the first case (Supplementary Figs. S2d and S3d), H₂O molecules lead to a rearrangement of this structure with time due to the ability of water to penetrate into the CM-D aggregate and thus to form strong hydrogen bonds with both cyanuric acid and melamine monomers to reach a thermodynamically more stable structure. In addition, the solubility of the monomers in water is sufficient to kinetically drive this reorganization (Supplementary Table S1). Hence, in the beginning the spheres swell slightly, and small rod-like crystals appear. Later on, the spherical aggregates collapse. In the second case (Fig. 1g), only the exposed interface between the aggregate and the second solvent (MeOH, EtOH and acetone) was changed with time. In this scenario, the less-polar solvent cannot penetrate into the “bulk-complex” due to the lower solubility of the monomers, but it can interact with the surface of aggregates. Consequently, the spherical shape was fully preserved within the experiment time (up to 20 h), and only the surface of the spherical aggregates is altered to a sheet- or stick-like morphology (further information is shown in Supplementary Figs. S5 and S6). Nevertheless, we note that this process is kinetically-driven and that the aggregates shape can be changed with sufficient reaction time (Supplementary Fig. S3d). However, in this work we focused mainly on the modified aggregates due to the preservation of their bulk shape.

3.2. Molecular dynamics simulations

In order to gain deeper understanding of the system at hand, all atom Molecular Dynamics (MD) Simulations were performed on the starting materials and the CM complex in all solvents (Fig. 2). Due to the limitations of the simulation, our model consists of CM aggregates with 18 solute molecules, thus, the small aggregates do not remain stable for long in any of the solvents investigated. Nevertheless, the lifetime of the larger clusters is significantly longer in acetone and EtOH than in the other solvents. The tendency for cluster formation of the molecules is obvious in the radial distribution functions (RDF) between cyanuric acid and melamine (Fig. 2a), which remains larger than one up to a distance of 1.2 nm in all solvents. However, the first coordination peak for acetone and EtOH,

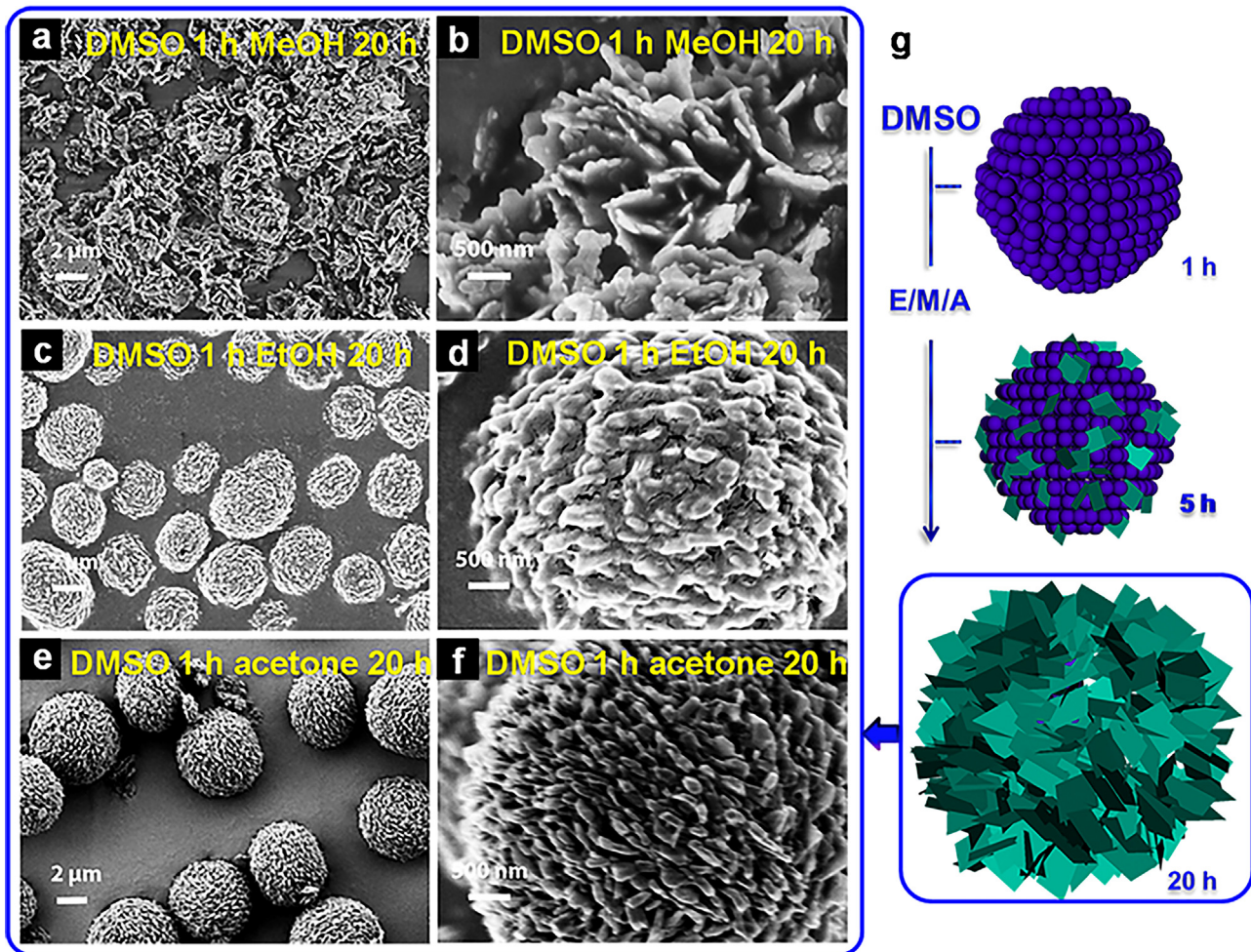


Fig. 1. Evolution of CM aggregate after formation in DMSO and treatment with less polar solvent (MeOH, EtOH, acetone, respectively). SEM images of CM-D1M20 (a,b), CM-D1E20 (c,d) and CM-D1A20 (e,f). (b,d,f) show larger magnification images of (a,c,e), respectively. (g) Scheme showing modification of CM aggregate transferred from DMSO to MeOH, EtOH and acetone.

is almost a factor 8 larger than for water, highlighting the stronger aggregation. Thenceforth, we studied the propensity of cyanuric acid-melamine complex and cyanuric acid to form hydrogen bonds with the solvent. The hydrogen bond data of the polar solvents listed in Fig. 2b and c is consistent with the solubility data, and with the different ability of the solvents to penetrate and restructure the spherical aggregates. For example, water forms more than three times as many hydrogen bonds with the solute molecules within the CM complex than acetone. Inversely, although the ordered aggregates have dissolved, many hydrogen bonds between solute molecules remain in acetone, whereas barely any are present in the water system. This trend highlights the ability of the water molecules to compete with hydrogen bonds within the crystal-structure, and thus to solvate these molecules much more easily than acetone. Another factor that can play a major role is the long range ordering effects of solvent molecules around the CM aggregate (Fig. 2d). Whereas, for water, there is no perceptible long range effect of the starting molecules beyond the first hydration shell, the RDFs for both acetone and EtOH, show three strong neighbor peaks in the RDFs indicating a much stronger ordering of the solvent to a distance of 1.5 nm. This suggests a larger solvation layer around the CM aggregate. Thus, the restructuration of the supramolecular complex in these solvents required additional energy in order to break the ordered solvation layer. Snapshots from the MD simulations are given in Supplementary Fig. S7.

3.3. Formation of C_3N_4 generated by CM condensation

In the interest of synthesizing photoactive carbon nitride, the CM aggregates were heated to 550 °C for 4 h under nitrogen atmosphere with a heating ramp of 2.3 °C min⁻¹. As confirmed by SEM images, the morphology of C_3N_4 (C_3N_4 s prepared from CM-D, CM-H, CM-M, CM-E and CM-A were labeled as CN-D, CN-H, CN-M, CN-E and CN-A, respectively) strongly depends on the solvent that was used for the formation of CM aggregates (Supplementary Fig. S8). In all cases, the starting structure is not fully preserved during the calcination process. In particular for CM-D, the sphere-like aggregates collapse during the heating, only fractures of the particle shell remain, and more irregular and open spheres morphologies are formed. The formation of C_3N_4 -like materials was confirmed by elemental analysis and electron energy loss spectroscopy (Supplementary Table S2 and Fig. S9). All samples have a C/N molar ratio of ~0.6 and contain less than 3% hydrogen, indicating that almost all NH₂ groups react during the condensation. Moreover, the sum of the proportions of carbon, nitrogen and hydrogen indicates a low amount of oxygen, showing that almost all the C=O groups in the cyanuric acid reacted with melamine to form C_3N_4 . Besides, FT-IR and XRD analysis also identified the C_3N_4 -like structure (Supplementary Fig. S10).

The CM aggregates which were first prepared in DMSO and afterwards modified by a second solvent treatment were also applied as carbon nitride precursors (C_3N_4 s prepared from CM-D1H20, CM-

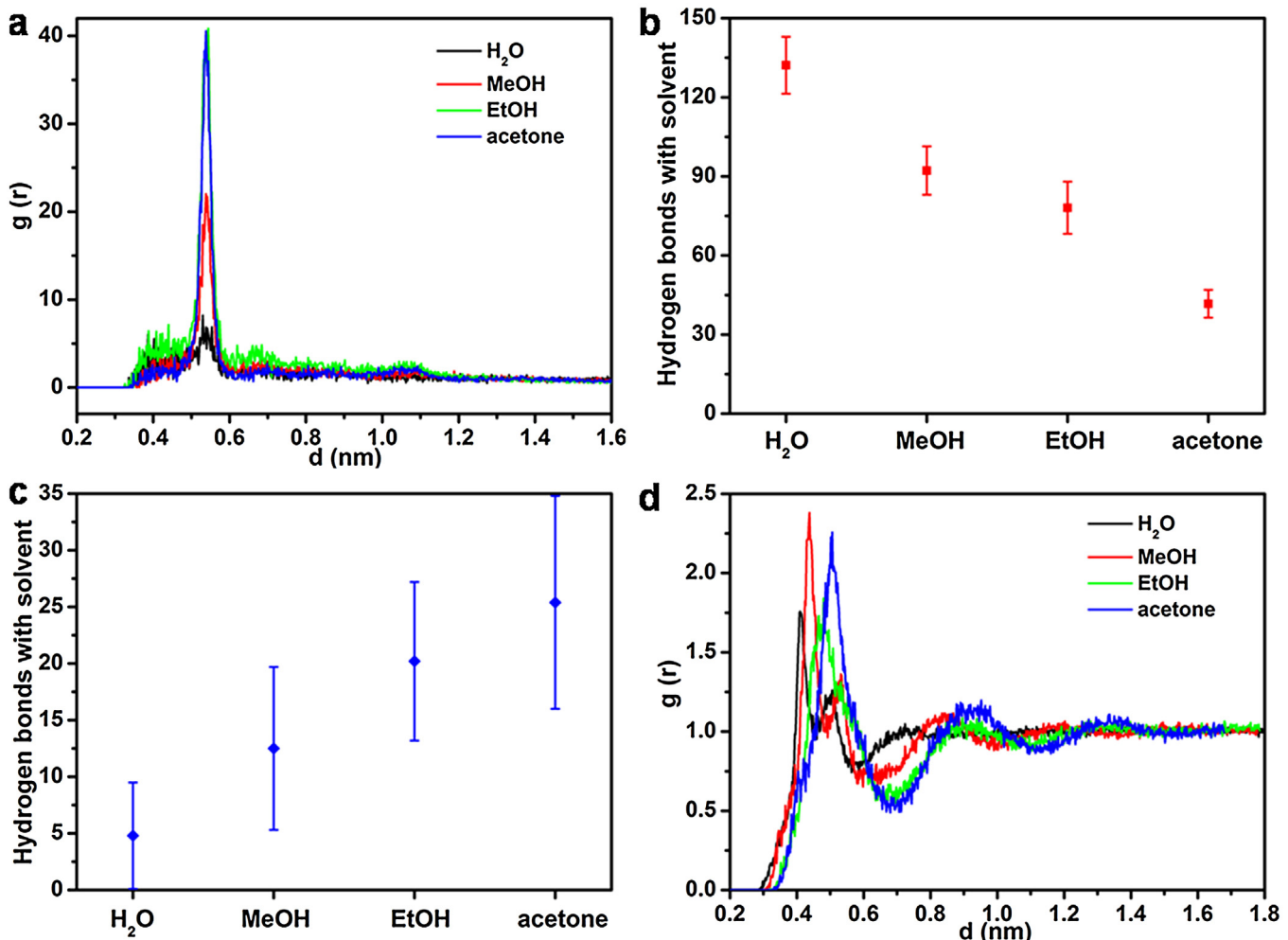


Fig. 2. Analysis of the MD trajectories. (a) RDF between cyanuric acid and melamine. (b) Average number of hydrogen bonds formed between the CM complex and the respective solvent. (c) Average number of hydrogen bonds formed between solute molecules within the complex in different solvents. Error bars represent one STD of the distribution. (d) RDF for solvent molecules from cyanuric acid.

D1M20, CM-D1E20 and CM-D1A20 were labeled as CN-DH, CN-DM, CN-DE and CN-DA, respectively). As expected, for the water system, due to the almost full reorganization of the CM aggregate, very similar C_3N_4 morphology as the one solely from water was achieved (Supplementary Fig. S11). On the contrary, the modification of only the CM-D surface by a less polar second solvent (MeOH, EtOH or acetone) resulted almost in a full preservation of the starting spherical morphology even after calcination at high temperatures (Fig. 3). Hollow sphere-like C_3N_4 particles with holes on the surface can be clearly seen in CN-DM and CN-DE. In the case of acetone treatment of the supramolecular assemblies, the morphology was even fully kept up to 550 °C, forming homogeneous C_3N_4 spheres.

Due to the unique morphology of the CN-DA particles, we will concentrate on the characterizations of CN-DA compared to CN-D in the remainder of this manuscript. To investigate the growth mechanism of the carbon nitride materials from the supramolecular precursors at high temperatures, *in-situ* heating experiments during optical microscopy (Supplementary Fig. S12) or inside a TEM (Supplementary Figs. S13 and S14, Fig. 4a–e) were conducted, respectively. In both samples, the supramolecular complexes exhibit platelets of hexagonal shape. For CM-D the morphology changes to a sheet-like structure. However, the heating experiments of the CN-DA show that in this case the spheres shrink and that the inner part diffuses toward the shell of the spheres (see Supplementary Fig. S14). High resolution imaging of the product

obtained after the heating experiment reveals a structure consisting of agglomerated, disordered and bent carbon nitride sheets (see Fig. 4e and EELS data in the Supplementary Fig. S9). A closer inspection of the morphological changes monitored during the *in-situ* heating in the microscope (Supplementary Fig. S14) discloses that individual hexagonally shaped platelets of the supramolecular structure preserve their shape up to around 500 °C. Thus, CN-DA preserves the sphere-like structure with higher material intensity in the outer part compare to the inner one (Fig. 4e inset). The electron beam dose was kept at a minimum in order to reduce beam-induced artifacts. Final comparison of structures that were followed during heating with structures that were not illuminated by the electron beam during the heating experiment did not show any detectable morphological differences.

Additional evidence for the formation of C_3N_4 was acquired by X-ray photoelectron spectroscopy (XPS) measurements of CN-DA. As shown in Fig. 4f,g, the N 1s peak in XPS spectrum can be resolved into three peaks centered at the binding energies of 398.6 eV, 400.3 eV and 401.3 eV, belonging to the C=N–C, N–(C)₃ and N–H₂ species, respectively [39]. The C 1s spectra of CN-DA can be constructed from a superposition of three peaks at 293.00 eV, 284.60 eV and 288.10 eV, corresponding to the π – π^* transition loss peak, sp² C=C bonds and to N=C–N species, respectively. Similar results were also observed with CN-D in Supplementary Fig. S8c,d.

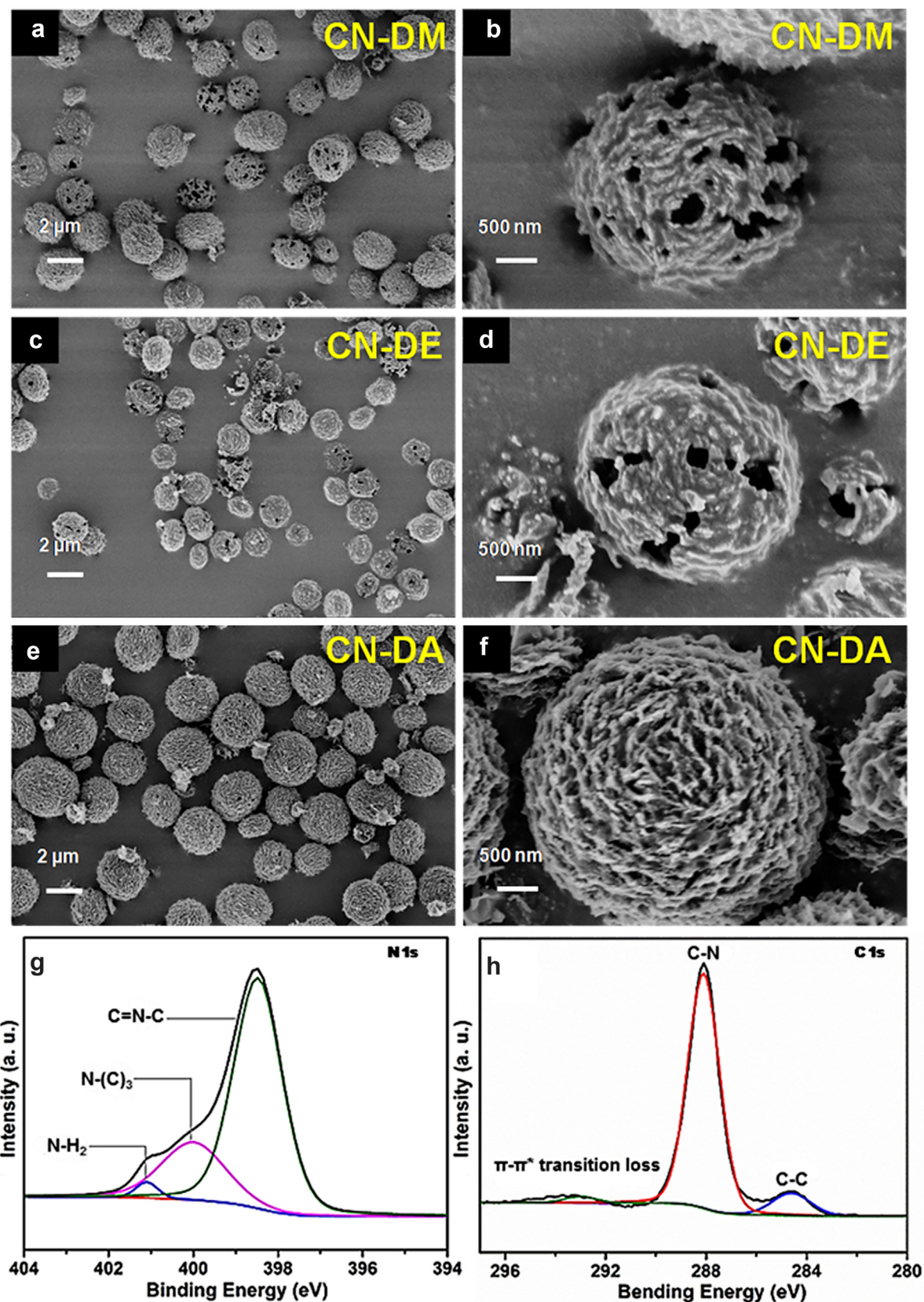


Fig. 3. Information of $\text{C}_3\text{N}_4\text{s}$ calcinated from CMs after a second solvent treatment. SEM images of CN-DM (a,b), CN-DE (c,d), CN-DA(e,f). (b,d,f) show larger magnification images of (a,c,e), respectively.

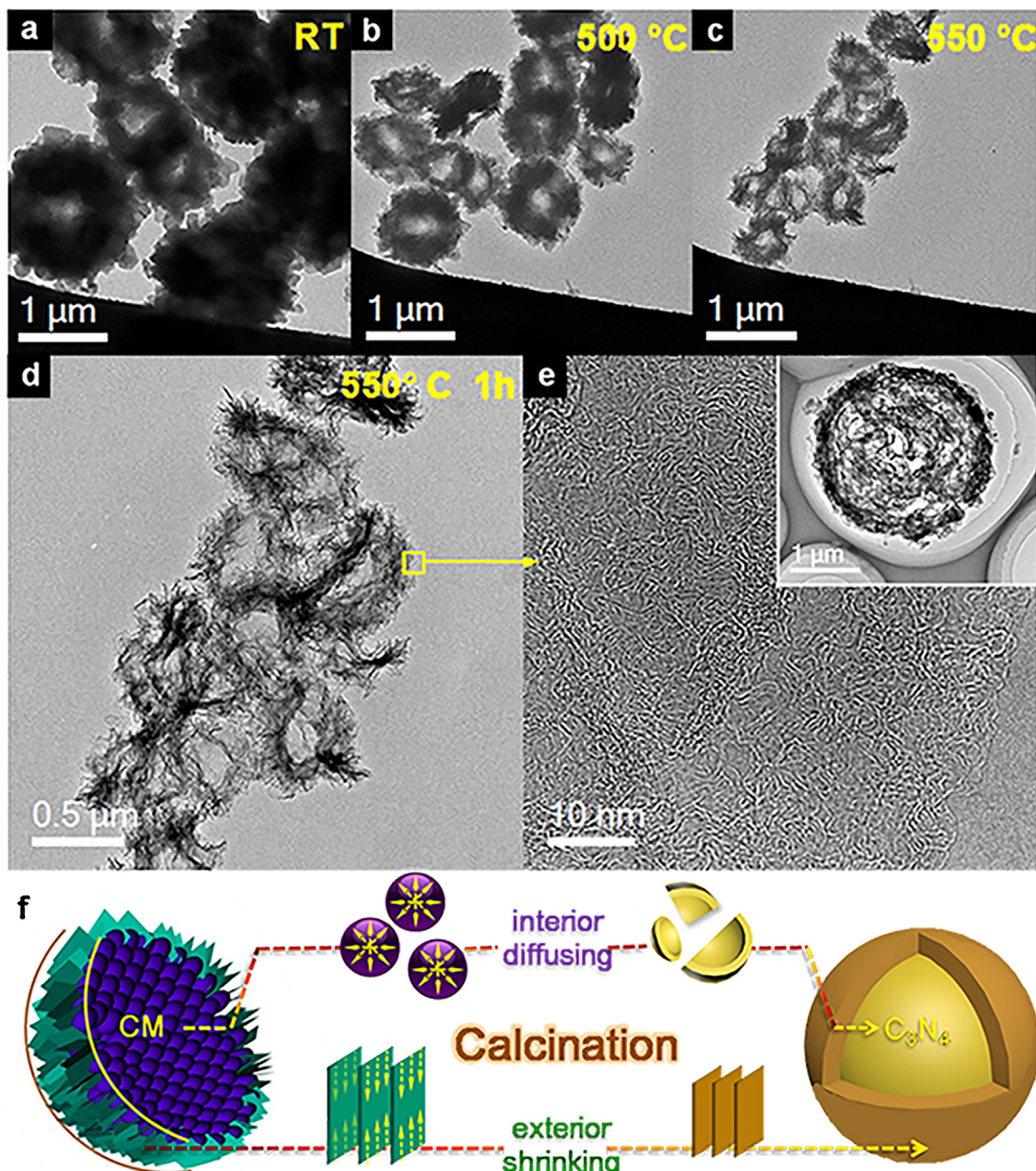


Fig. 4. Structural evolution of CM-DA during heating up to 550 °C. TEM images of CM-DA at room temperature (a), during heating at 500 °C (b) and 550 °C (c) and after keeping the temperature at 550 °C for another 1 h (d,e). Inset is the TEM image of CN-DA after calcination. (f,g) N 1s and C 1s core-level XPS spectra of CN-DA. (h) Mechanism of the formation of sphere-like C₃N₄ from CM aggregates (CM-DM, CM-DE or CM-DA).

These assignments are in good agreement with the EELS data and previous investigations of carbon nitride [39].

Based on the above, we assume that the preservation of the starting morphology is due to the formation of two different CM supramolecular crystals with altered strength of hydrogen bonds which react differently upon heating (Fig. 4f). As shown before (Fig. 1) the second solvent treatment of CM aggregates results in the modification of the surface structures compared to the bulk. In addition, due to the surface reorganization of the CM aggregates in the presence of a less polar solvent compared to the initial DMSO, the hydrogen bonds between cyanuric acid and melamine become stronger. Hence, upon heating the two crystals may possess different diffusion rates and melting properties [39,40]. In addition, the stronger hydrogen-bonds between cyanuric acid and melamine in the outer layer compared to the inner part of the supramolecular

aggregates may help to prevent the overall structure from collapsing at high temperatures.

3.4. Photocatalytic behaviors of carbon nitride materials

In order to evaluate the photoactivity of all the carbon nitride materials compared to pristine C₃N₄ (calcinated from melamine), we measured the hydrogen evolution in a water/triethanolamine (TEOA) solution with Pt as co-catalyst under white light illumination (Fig. 5a). Very interestingly, all carbon nitride materials that were synthesized by sequential two-solvent treatment demonstrated more than two times higher photoactivity compared to the carbon nitride from the single solvent system. Moreover, the hydrogen production of the best C₃N₄ photocatalyst is approximately ten times as high as the hydrogen production from bulk C₃N₄ (the one

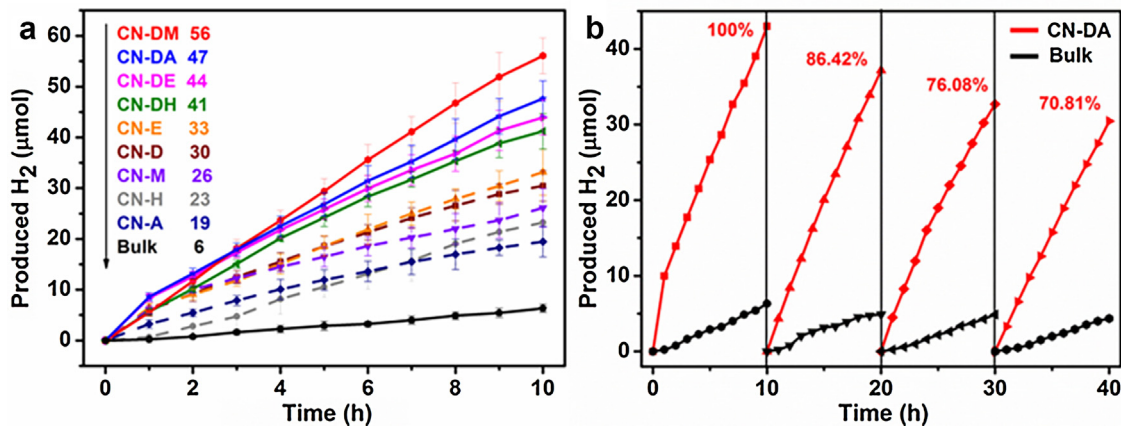


Fig. 5. Photocatalytic H₂ production. (a) Time courses of H₂ production from water under white LED irradiation, the error bars stand for 3 different measurements. (b) Cycling measurements of H₂ generation of CN-DA and bulk (carbon nitride calcinated from melamine).

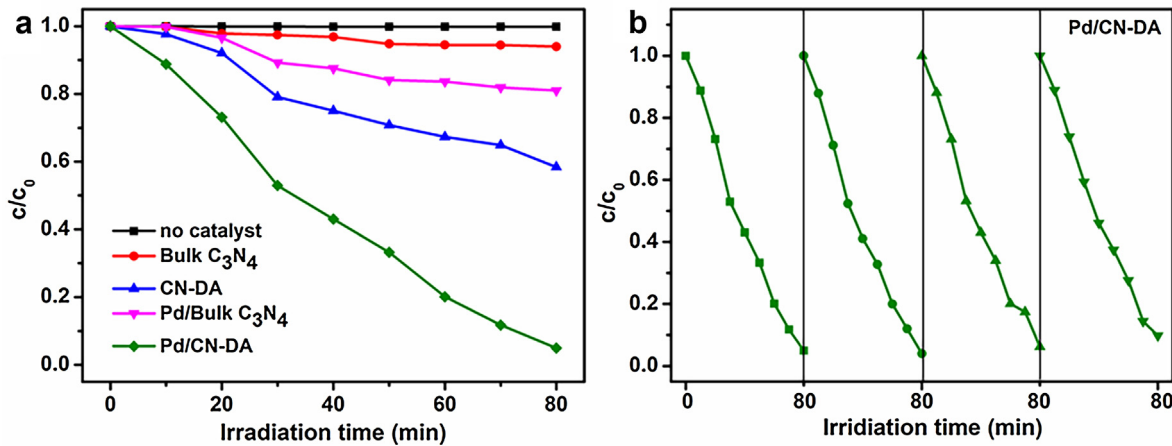


Fig. 6. CN-DA photoactivity on p-NP degradation under UV light. (a) p-NP degradation on differing C₃N₄. (b) Cycling measurements of Pd/CN-DA.

that was prepared from melamine only as a precursor). In addition, the CN-DA shows AQY of 0.96%, measured by monochromatic LED lamps with band pass filter of 420 ± 4.6 . The stability of the new formed C₃N₄ was investigated with four consecutive runs of the photocatalytic reaction (for simplicity, we show here only CN-DA), maintaining more than 70% of the initial activity after 40 h (Fig. 5b, Supplementary Fig. S15), demonstrating good chemical and photophysical stability. Moreover, the sphere-like morphology of CN-DA was fully preserved (Supplementary Fig. S16), indicating the recyclability of the catalyst.

The superior catalytic activity of CN-DA was further demonstrated by the degradation of RhB and p-nitrophenol (p-NP). As shown in Supplementary Fig. S17, CN-DA exhibited the highest photocatalytic activity, especially in the first 20 min. Fig. 6 and Supplementary Fig. S18 show the degradation of p-NP, which is considered to be much more stable than the organic dyes. Already in the absence of co-catalyst, CN-DA photodegraded ~50% after only 80 min, while the bulk-C₃N₄ showed negligible activity. After the addition of 5 wt% Pd as co-catalyst, the degradation was completed in 80 min. It is worth mentioning that the bulk-C₃N₄/Pd showed lower activity even compared to the bare CN-DA. In addition, the CN-DA maintained more than 90% of the initial activity during 4 sequential cycles.

In general, the photocatalytic activity depends on the surface area (active catalytic sites), optical absorption (light harvesting properties) and on the photophysical properties of the photocatalyst, i.e., the increase of the life time of electrons and holes under

illumination by the creation of defects sites, heterojunction and more. From the absorption spectra (Fig. 7a) and the hydrogen evolution rates, we can estimate that the light harvesting properties was not the crucial reason for the photoactivity improvement. In order to determine whether the surface area or the electronic properties are responsible for the high activity, we plot the hydrogen evolution rate as a function of the surface area in Fig. 7b. In general, the surface area is related to a material's photoactivity due to the increased number of active sites for the reaction. Such a rough trend is observable also for our materials. However, most of the carbon nitrides exhibit different photoactivity for similar surface areas (for example, compare the different H₂ evolution for materials with a surface area of roughly 70 m² g⁻¹, which differs by a factor of more than two).

Photoluminescence (PL) is very useful technique to investigate the charge transfer properties of the given photocatalysts. As shown in Fig. 7c, the fluorescence of CN-D and CN-DA is quenched compared to the pristine C₃N₄. Moreover, the introduction of acetone in the synthetic procedure (CN-DA) results in increased fluorescence quenching. The quenching of the emission intensity indicates that the relaxation of a fraction of photocarriers occurs via a non-radiative pathway, presumably through charge transfer of electrons and holes to new localized/surface states.

From these observations we can carefully estimate that enhanced photoactivity is mainly due to the alteration of the electronic properties. Combining the influence of the second solvent on chemical and photophysical properties and the high photoac-

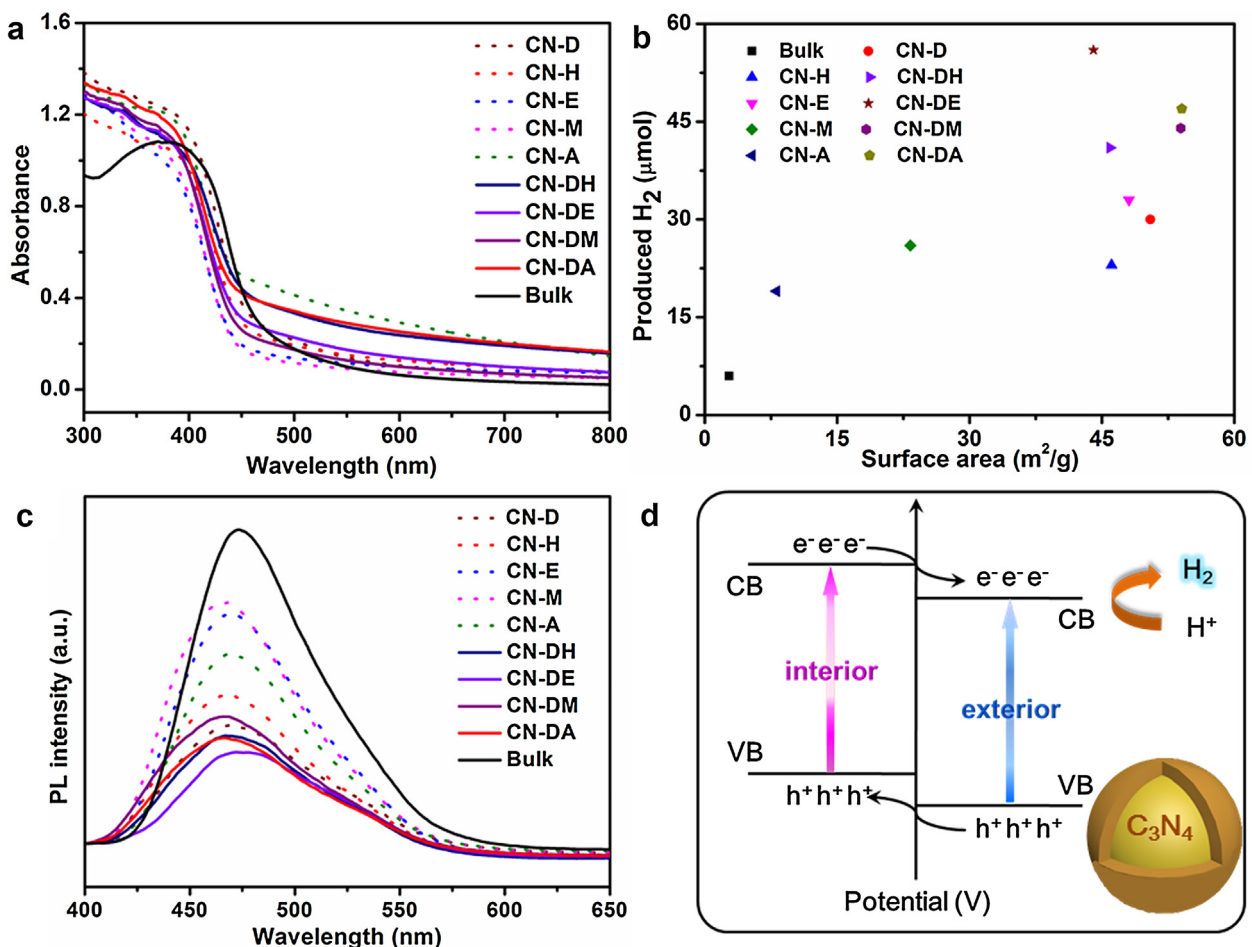


Fig. 7. (a) UV-vis absorbance of differing C_3N_4 catalysts. (b) H_2 production vs. the surface area. (c) PL spectra of differing C_3N_4 catalysts. (d) Conceptual scheme of photocatalytic progress on carbon nitride materials (CN-DM, CN-DE, CN-DA).

tivity of carbon nitride materials, we propose that the differences between the starting CM crystals in the shell of spherical assemblies result in the formation of C_3N_4 with a gradient in the position of energy levels, i.e., valence (VB) and conduction band (CB) (Fig. 7d). The preservation of the spherical structure in the final C_3N_4 suggests that the outer crystals in the CM-DA are thermodynamically more stable compared to the inner crystals. Due to these differences, the outer C_3N_4 is supposed to possess energy bands which are slightly downshifted compare to the inner layer, forming a heterojunction structure which further improves the charge separation process. Thus, the introduction of sequential two-solvent treatment as a modifier of supramolecular assemblies leads not only to precise control of the carbon nitride structure but to the alteration of the photophysical and catalytic properties.

4. Conclusions

In conclusion, we demonstrated a new, facile and efficient “template-free” method to synthesize highly ordered carbon nitride materials with controllable photophysical and catalytic properties, simply via the alteration of the morphology of starting supramolecular precursors by different solvents. The kinetic and thermodynamic roles of sequential two-solvent treatment on the supramolecular aggregates were experimentally and theoretically studied. We showed that sequential solvent introduction can lead to a full structural rearrangement or only to the modification of the outer shell of supramolecular aggregates by the creation of a gradient in hydrogen bonds interaction strength across the aggregate.

In-situ HRTEM measurements revealed that the surface modification of the starting supramolecular complexes leads to a different mechanism of material growth at high temperatures. Using these modified cyanuric acid-melamine aggregates as the carbon nitride precursor leads to the formation of hollow spheres with superior photocatalytic activity. This work opens the possibilities for the facile synthesis of many catalytic materials with the possibility to design their final properties already on the monomer level. Moreover, our findings significantly improve our understanding on the role of the solvent in supramolecular self-assembly alongside the mechanism behind high temperature reactions.

Acknowledgements

We thank Prof. Markus Antonietti and, Dr. Davide Esposito for fruitful discussion. We would also like to thank the technical staff at MPIKG and our group members for performing service measurements such as SEM, elemental analysis. This work was supported by NSF of China (No. 51572125), the Fundamental Research Funds for the Central Universities (Nos. 20915011311, 30916014103) and PAPD of Jiangsu.

Appendix A. Supplementary data

Supplementary data associated with this article can be found, in the online version, at <http://dx.doi.org/10.1016/j.apcatb.2016.12.030>.

References

- [1] M.A. Mateos-Timoneda, M. Crego-Calama, D.N. Reinhoudt, *Chem. Soc. Rev.* 33 (2004) 363–372.
- [2] D.C. Sherrington, K.A. Taskinen, *Chem. Soc. Rev.* 30 (2001) 83–93.
- [3] A.G. Slater, L.M.A. Perdigao, P.H. Beton, N.R. Champness, *Acc. Chem. Res.* 47 (2014) 3417–3427.
- [4] T. Bisheti, B. Garg, S. Murat, S. Chauhan, *J. Inclusion Phenom. Macrocycl. Chem.* 78 (2014) 103–111.
- [5] Y.-S. Jun, E.Z. Lee, X. Wang, W.H. Hong, G.D. Stucky, A. Thomas, *Adv. Funct. Mater.* 23 (2013) 3661–3667.
- [6] Y. Liao, S. Zhu, J. Ma, Z. Sun, C. Yin, C. Zhu, X. Lou, D. Zhang, *ChemCatChem* 6 (2014) 3419–3425.
- [7] X.B. Shao, X.K. Jiang, S.Z. Zhu, Z.T. Li, *Tetrahedron* 60 (2004) 9155–9162.
- [8] M. Shalom, S. Inal, C. Fettkenhauer, D. Neher, M. Antonietti, *J. Am. Chem. Soc.* 135 (2013) 7118–7121.
- [9] S. Yagai, *J. Photoch. Photobio. C* 7 (2006) 164–182.
- [10] X. Wang, K. Maeda, A. Thomas, K. Takanabe, G. Xin, J.M. Carlsson, K. Domen, M. Antonietti, *Nat. Mater.* 8 (2009) 76–80.
- [11] H. Li, Y. Liu, X. Gao, C. Fu, X. Wang, *ChemSusChem* 8 (2015) 1189–1196.
- [12] J. Xu, T.J.K. Brenner, L. Chabanne, D. Neher, M. Antonietti, M. Shalom, *J. Am. Chem. Soc.* 136 (2014) 13486–13489.
- [13] H. Wang, X. Yuan, Y. Wu, G. Zeng, X. Chen, L. Leng, H. Li, *Appl. Catal. B-Environ.* 174 (2015) 445–454.
- [14] Q. Han, F. Zhao, C. Hu, L. Lv, Z. Zhang, N. Chen, L. Qu, *Nano Res.* 8 (2015) 1718–1728.
- [15] J. Sun, Y. Fu, G. He, X. Sun, X. Wang, *Appl. Catal. B-Environ.* 165 (2015) 661–667.
- [16] C. Han, Y. Wang, Y. Lei, B. Wang, N. Wu, Q. Shi, Q. Li, *Nano Res.* 8 (2015) 1199–1209.
- [17] T.J. Prior, J.A. Armstrong, D.M. Benoit, K.L. Marshall, *CrystEngComm* 15 (2013) 5838–5843.
- [18] A. Thomas, F. Goettmann, M. Antonietti, *Chem. Mater.* 20 (2008) 738–755.
- [19] Y. Wang, J. Zhang, X. Wang, M. Antonietti, H. Li, *Angew. Chem. Int. Ed.* 49 (2010) 3356–3359.
- [20] Z.P. Chen, M. Antonietti, D. Dontsova, *Chem. Eur. J.* 21 (2015) 10805–10811.
- [21] J. Sun, J. Zhang, M. Zhang, M. Antonietti, X. Fu, X. Wang, *Nat. Commun.* 3 (2012) 1139–1145.
- [22] Y.D. Yin, R.M. Rioux, C.K. Erdonmez, S. Hughes, G.A. Somorjai, A.P. Alivisatos, *Science* 304 (2004) 711–714.
- [23] H.J. Fan, M. Knez, R. Scholz, K. Nielsch, E. Pippel, D. Hesse, M. Zacharias, U. Goesele, *Nat. Mater.* 5 (2006) 627–631.
- [24] Y.-S. Jun, J. Park, S.U. Lee, A. Thomas, W.H. Hong, G.D. Stucky, *Angew. Chem. Int. Ed.* 52 (2013) 11083–11087.
- [25] M. Shalom, M. Guttentag, C. Fettkenhauer, S. Inal, D. Neher, A. Llobet, M. Antonietti, *Chem. Mater.* 26 (2014) 5812–5818.
- [26] Y. Ishida, L. Chabanne, M. Antonietti, M. Shalom, *Langmuir* 30 (2014) 447–451.
- [27] I.S. Choi, X.H. Li, E.E. Simanek, R. Akaba, G. Whitesides, *Chem. Mater.* 11 (1999) 684–690.
- [28] C.T. Seto, G.M. Whitesides, *J. Am. Chem. Soc.* 115 (1993) 905–916.
- [29] L.D. Williams, B. Chawla, B.R. Shaw, *Biopolymers* 26 (1987) 591–603.
- [30] C. Oostenbrink, A. Villa, A.E. Mark, W.F.V. Gunsteren, *J. Comput. Chem.* 25 (2004) 1656–1676.
- [31] A. Vishnyakov, A.P. Lyubartsev, A. Laaksonen, *J. Phys. Chem. A* 105 (2001) 1702–1710.
- [32] T.J. Prior, J.A. Armstrong, D.M. Benoit, K.L. Marshall, *CrystEngComm* 15 (2013) 5838–5843.
- [33] D.V.D. Spoel, E. Lindahl, B. Hess, G. Groenhof, A.E. Mark, H.J.C. Berendsen, *J. Comput. Chem.* 26 (2005) 1701–1718.
- [34] T. Darden, D. York, L. Pedersen, *J. Chem. Phys.* 98 (1993) 10089–10092.
- [35] B. Hess, H. Bekker, H.J. Berendsen, J.G. Fraaije, *J. Comput. Chem.* 18 (1997) 1463–1472.
- [36] S. Miyamoto, P.A. Kollman, *J. Comput. Chem.* 13 (1992) 952–962.
- [37] H. Xu, J. Yan, Y. Xu, Y. Song, H. Li, J. Xia, C. Huang, H. Wan, *Appl. Catal. B-Environ.* 129 (2013) 182–193.
- [38] B.V. Lotsch, M. Döblinger, J. Sehnert, L. Seyfarth, J. Senker, O. Oeckler, W. Schnick, *Chem. Eur. J.* 13 (2017) 4969–4980.
- [39] X. Yang, H. Tang, J. Xu, M. Antonietti, M. Shalom, *ChemSusChem* 8 (2015) 1350–1358.
- [40] W. Wang, M. Dahl, Y. Yin, *Chem. Mater.* 25 (2013) 1179–1189.